

MIT Open Access Articles

Analytical Maneuver Library for Remote Inspection with an Underactuated Spacecraft

The MIT Faculty has made this article openly available. **Please share** how this access benefits you. Your story matters.

Citation: Jia-Richards, Oliver and Lozano, Paulo C. 2022. "Analytical Maneuver Library for Remote Inspection with an Underactuated Spacecraft." *Journal of Guidance, Control, and Dynamics*, 45 (4).

As Published: 10.2514/1.g005766

Publisher: American Institute of Aeronautics and Astronautics (AIAA)

Persistent URL: <https://hdl.handle.net/1721.1/141641>

Version: Author's final manuscript: final author's manuscript post peer review, without publisher's formatting or copy editing

Terms of use: Creative Commons Attribution-Noncommercial-Share Alike



An Analytical Maneuver Library for Remote Inspection with an Underactuated Spacecraft

Oliver Jia-Richards¹ and Paulo C. Lozano²

Massachusetts Institute of Technology, Cambridge, Massachusetts, 02139

This paper presents an analytical library for maneuvering of an underactuated spacecraft around a central target with application to remote inspection. Free-flying small spacecraft are an attractive option for *in situ* remote inspection but require maneuvering strategies that are computationally simple, such that they can be implemented on a small spacecraft computer, while still allowing for constraints like plume impingement and underactuation to be included. An analytical maneuver library provides a sub-optimal solution but can be computed without the need for numerical optimization. In addition, the low fuel cost of maneuvers means that the degree of sub-optimality of the analytical maneuvers is marginal. To develop the library, forced circular motion is used in order to place the spacecraft in a controllable state such that external disturbances can be rejected. From there, maneuvers can be designed in order to manipulate the circular motion and accomplish maneuvers such as joining the circular motion from rest or changing the circle's radius. Conditions under which plume impingement is guaranteed to be avoided are developed and applications of the maneuver library to point-to-point maneuvering and landing on/docking to a rotating target are shown.

I. Introduction

Remote inspection of spacecraft allows for an assessment of the condition of the vehicle's exterior and can be conducted with ground-based instruments or in proximity to the spacecraft. While not

¹ Doctoral Candidate, Department of Aeronautics and Astronautics, oliverjr@mit.edu, Student Member AIAA

² Professor, Department of Aeronautics and Astronautics, plozano@mit.edu, Associate Fellow AIAA

commonly used, remote inspection can be used to determine the health of high-value spacecraft such as those with astronauts on board or to assess a piece of debris prior to attempting to capture it. As the probability of returning astronauts to the Moon or sending them to deep space increases along with the advancement of technologies for active debris removal, the ability to perform remote inspection of other spacecraft becomes more and more valuable.

Different methodologies for remote inspection can be compared based on their ability to provide coverage of the exterior surface of the target object, the spatial resolution which can be achieved, as well as their overall risk [1]. Of all the available methods, inspection with a free-flying small spacecraft is a highly attractive option due to its ability to provide good coverage and spatial resolution while not incurring significant risk in terms of cost or human involvement. These free-flying inspectors could either be launched from the target spacecraft, if for instance the target spacecraft is a space station, or rendezvous with the target, if the target is a piece of debris.

At the most basic level, remote inspection with a free-flying small spacecraft can be conducted with a simple micro-spacecraft designed for short-term inspection of a target vehicle. Passive CubeSats for spacecraft inspection have been proposed where the spacecraft contains no actuation system [1]. This method minimizes many of the risks associated with free-flying spacecraft, but cannot provide good coverage of the entire exterior of the target without requiring the use of multiple inspector spacecraft, has limited inspection time before it drifts too far away from the target, and is not applicable to uncooperative targets such as debris.

A step above the passive approach is to outfit the inspector spacecraft with a simple cold-gas propulsion system. The high thrust density of cold-gas propulsion, relative to other miniaturized propulsion technologies, means that nozzles can be placed along each axis of the spacecraft in order to provide linear position dynamics. The guidance systems for these spacecraft are often quite straightforward and rely on the linear dynamics in order to simplify the control strategy. Point-to-point maneuvering, where the spacecraft is simply provided a series of waypoints, is the most basic maneuvering strategy [2]. For targets around a large central body, such as Earth, the natural orbital dynamics can be leveraged in order to create trajectories based on a series of impulsive maneuvers [3]. Alternatively, the spacecraft can be forced into a circumnavigating trajectory around the target

which costs more propellant, but allows for finer control over the maneuver [4]. More complex maneuvers that use both natural and forced motion can be devised that take into account further constraints such as maintaining illumination from the Sun on the solar panels [5].

These methodologies are appealing due to their simplicity. However, while the maneuvers based in natural orbit motion leverage the dynamics to save fuel and avoid plume impingement, they are also at the mercy of those same natural dynamics. In particular, the period of the circumnavigating inspection trajectories will be the same as the orbital period of the target. For targets in low-Earth orbit this might be acceptable as orbital periods are around 90 minutes. However, in geostationary orbit the orbital period rises to a day and in deep space the orbital period is on the order of years. Clearly, for maneuvering strategies that are applicable to scenarios beyond low-Earth orbit, forced motion is required. The forced circular motion of Ref. [4] is a promising start, but the range of developed maneuvers is limited and is constrained to fully-actuated systems.

Beyond the desire to increase the number of possible maneuvers, it may also be desired to use propulsion systems other than cold-gas propulsion. The low efficiency of cold-gas propulsion restricts its use to missions with low maneuvering requirements. In particular, cold-gas propulsion could not be used for a reconnaissance spacecraft that travels between multiple pieces of debris or for long-duration inspection missions where the inspector spacecraft is required to be active over the course of several months. While cold-gas propulsion dominates the list of CubeSat-compatible propulsion systems with flight heritage, other propulsion technologies are being developed that could resolve this issue [6]. One such example is microfabricated electrospray propulsion [7–9] which has the potential to provide relatively high thrust density while also not requiring significant amounts of power. These types of thrusters have also been demonstrated in a laboratory environment for control of a CubeSat-like test vehicle [10].

The use of propulsion systems other than cold-gas propulsion, such as electrospray propulsion, creates other challenges for the maneuvering of a free-flying inspector, many of which are covered in Ref. [11]. The exhaust of chemical and electric propulsion systems can be reactive and contaminate any surfaces that they impinge on [12, 13]. Furthermore, due to low thrust density and challenges associated with placing thrusters along multiple axes, the thrust axis for the propulsion system is

usually fixed with respect to the spacecraft body causing the spacecraft to be underactuated - the direction of the thrust vector is tied to the spacecraft's attitude and cannot be independently set. Therefore, maneuvering methodologies should also be able to handle plume impingement constraints as well as underactuated spacecraft.

For a more expansive set of maneuvers that can handle constraints such as plume impingement and underactuation, mathematical programming, where the trajectory planning process is expressed as a constrained optimization, is typically used. Mixed-integer linear programming allows for a trajectory to be planned that can account for multiple different types of discrete constraints such as plume impingement [14] or that the trajectory always be passively safe [15]. However, this formulation requires that the spacecraft not be underactuated in order to ensure that the dynamics remain linear. Methods that enable continuous constraint satisfaction have also been explored, but for impulsive maneuvers [16].

Approaches within model-predictive control use quadratic programming to penalize changes to the thrust vector in order to accommodate underactuated spacecraft while avoiding the use of nonlinear programming [17]. However, this approach also places a cost on changes to the thrust magnitude where only the thrust direction should be penalized. Minimization of plume impingement is also considered in Ref. [17] by constraining the allowed thrust in the direction of the target as the inspection spacecraft approaches which could alleviate structural loading concerns but does not prevent surface contamination. Plume impingement has also been considered as a soft constraint by including it in the objective function [18]. However, this approach requires nonlinear programming, and the computational cost of accounting for plume impingement this way is found to be prohibitive.

For mathematical programming and model-predictive control approaches as well as any other approaches that require numerical optimization, there is a secondary cost that is usually not considered. Typically, the goal of the optimization is to minimize the fuel cost of the trajectory, thereby implicitly maximizing the available mass for payload or the number of maneuvers that can be accomplished. However, the computational cost of performing nonlinear optimization is beyond the capabilities of current small spacecraft computers. As such, in order to implement these methods, more powerful computers are required which in turn requires more power and a larger power system.

As will be shown in Section III, the fuel cost for basic inspection maneuvers will be on the order of 1-10 mg. Therefore, it is very likely that the increase in mass for better computation and power systems will outweigh any fuel savings gained by optimizing the trajectory.

A comparison of the maneuvering methods developed for actual spacecraft, such as [1–4], and methods developed in theory, such as [14–18], show that a technology gap exists between the two. The former are compatible with small-spacecraft computers but lack applicability for more complex maneuvering or spacecraft architectures while the latter expand the possible maneuvers and architectures but are incompatible with small-spacecraft computers. Methodologies that are able to bridge this gap are required in order to open up the use of high-efficiency propulsion, such as electric propulsion, for use during autonomous remote inspection.

This paper presents an analytical library for maneuvering an underactuated spacecraft around a target for remote inspection. An analytical maneuver library allows for a wide range of inspection missions to be accomplished while avoiding the secondary costs associated with numerical optimization, thereby permitting their implementation on small spacecraft. Section II motivates the use of forced circular motion around the target in order to allow the inspector spacecraft to control its position in the presence of external disturbances. Section III shows that the fuel mass required for basic inspection maneuvers will be small, thereby demonstrating that any optimization of the trajectory will be marginal. Section IV develops the maneuver library and Section V shows the conditions under which plume impingement on the target is guaranteed to be avoided. Finally, Section VI shows examples of how the maneuver library can be used in various mission scenarios.

II. Spacecraft Controllability

Figure 1 shows a notional spacecraft which operates in a two-dimensional world. The spacecraft has a propulsion system capable of producing thrust in the positive y_b direction and a reaction wheel capable of producing torques along the z axis. The dynamics of the spacecraft are given by

$$\ddot{x} = \frac{F}{m} \sin \phi \quad (1)$$

$$\ddot{y} = -\frac{F}{m} \cos \phi \quad (2)$$

$$\ddot{\phi} = \frac{\tau}{I} \quad (3)$$

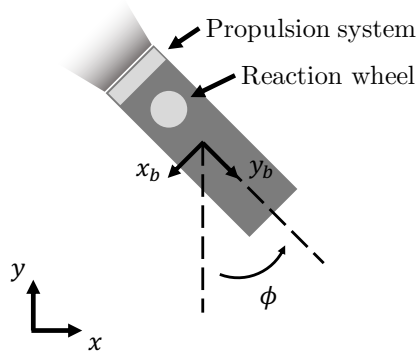


Fig. 1 Notional spacecraft

where F is the thrust produced by the propulsion system, m is the spacecraft's mass, ϕ is the spacecraft's heading measured anticlockwise from the negative- y direction, τ is the torque produced by the reaction wheel, and I is the rotational inertia of the spacecraft about the z axis.

Defining

$$v_x \equiv \dot{x}; \quad v_y \equiv \dot{y}; \quad \omega \equiv \dot{\phi} \quad (4)$$

then equilibrium in the inertial frame is given by $v_x = v_y = 0$, $\omega = 0$ as well as zero control input, $F = 0$ and $\tau = 0$. Linearizing the system about a heading, ϕ_0 , then the linearized dynamics are given by

$$\begin{bmatrix} \dot{x} \\ \dot{y} \\ \dot{v}_x \\ \dot{v}_y \\ \dot{\phi} \\ \dot{\omega} \end{bmatrix} = \begin{bmatrix} 0 & 0 & 1 & 0 & 0 & 0 \\ 0 & 0 & 0 & 1 & 0 & 0 \\ 0 & 0 & 0 & 0 & 0 & 0 \\ 0 & 0 & 0 & 0 & 0 & 0 \\ 0 & 0 & 0 & 0 & 0 & 1 \\ 0 & 0 & 0 & 0 & 0 & 0 \end{bmatrix} \begin{bmatrix} x \\ y \\ v_x \\ v_y \\ \phi \\ \omega \end{bmatrix} + \begin{bmatrix} 0 & 0 \\ 0 & 0 \\ \frac{\sin \phi_0}{m} & 0 \\ -\frac{\cos \phi_0}{m} & 0 \\ 0 & 0 \\ 0 & \frac{1}{I} \end{bmatrix} \begin{bmatrix} F \\ \tau \end{bmatrix} \quad (5)$$

The controllability matrix for this system, M_c , is given by

$$M_c = \begin{bmatrix} B & AB & A^2B & \dots & A^5B \end{bmatrix} \quad (6)$$

$$= \begin{bmatrix} 0 & 0 & \frac{\sin \phi_0}{m} & 0 & 0 & \dots & 0 \\ 0 & 0 & -\frac{\cos \phi_0}{m} & 0 & 0 & \dots & 0 \\ \frac{\sin \phi_0}{m} & 0 & 0 & 0 & 0 & \dots & 0 \\ 0 & -\frac{\cos \phi_0}{m} & 0 & 0 & 0 & \dots & 0 \\ 0 & 0 & 0 & \frac{1}{I} & 0 & \dots & 0 \\ 0 & \frac{1}{I} & 0 & 0 & 0 & \dots & 0 \end{bmatrix} \quad (7)$$

Since the controllability matrix only has four independent columns, it is rank deficient and the linearized system is not controllable. Intuitively, the spacecraft cannot respond to any disturbances along the x_b axis as neither modulating the propulsion system thrust nor rotating the spacecraft will produce a force along the x_b axis on their own. It is worth noting that modulating the thrust and rotating the spacecraft simultaneously would produce a force along the x_b axis but is not a linear response.

The system as defined has further complications beyond just being uncontrollable along the x_b axis. Since the propulsion system is unable to produce negative thrust, the spacecraft will not be able to respond to disturbances in the positive y_b direction. Both the controllability and negative thrust problems would be solved if in the equilibrium state the propulsion system is required to produce a positive thrust. This is possible if the spacecraft uses its propulsion system to place itself in a circular orbit around the target as shown in Figure 2. In this case, the spacecraft orbits around the target with constant radius r and angular frequency Ω with the required centripetal acceleration, $r\Omega^2$, being provided by the propulsion system.

The position dynamics for a frame centered on the target, instantaneously aligned with the inertial frame, but rotating with constant angular frequency $\vec{\Omega}$ can be calculated from

$$\vec{a}_i = \vec{a}_r + 2\vec{\Omega} \times \vec{v}_r + \vec{\Omega} \times (\vec{\Omega} \times \vec{r}_r) \quad (8)$$

where \vec{a} is acceleration, \vec{v} is velocity, and \vec{r} is position. Subscript i corresponds to coordinates in the instantaneously-aligned inertial frame while subscript r corresponds to coordinates in the rotating

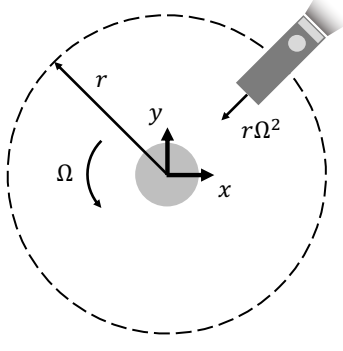


Fig. 2 Circular orbit used to allow for position control with linear control methods.

frame. The rotational dynamics of the spacecraft are unaffected by the coordinate transformation.

Assuming that the only accelerations in the inertial frame are from the propulsion system

$$\vec{a}_i = \frac{F}{m} \begin{bmatrix} \sin \phi \\ -\cos \phi \\ 0 \end{bmatrix} \quad (9)$$

and that the angular frequency of the rotating frame is in the positive z direction

$$\vec{\Omega} = \begin{bmatrix} 0 \\ 0 \\ \Omega \end{bmatrix} \quad (10)$$

with constant magnitude Ω , then the dynamics in the x - y plane of the rotating frame are

$$\ddot{x}_r = \Omega^2 x_r + 2\Omega v_{y,r} + \frac{F}{m} \sin \phi \quad (11)$$

$$\ddot{y}_r = \Omega^2 y_r - 2\Omega v_{x,r} - \frac{F}{m} \cos \phi \quad (12)$$

$$\ddot{\phi} = \frac{\tau}{I} \quad (13)$$

Equilibrium in this rotating frame is again given by $v_{x,r} = v_{y,r} = 0$ and $\omega = 0$ along with $\tau = 0$.

However, for a given position in the rotating frame, the equilibrium input thrust is now

$$F^* = m\Omega^2 \sqrt{x_r^2 + y_r^2} \quad (14)$$

with equilibrium heading

$$\phi^* = \tan^{-1} \left(-\frac{x_r}{y_r} \right) \quad (15)$$

Picking the equilibrium position to be $x_r = 0$ and $y_r = r_d$ where r_d is the desired orbital radius, then the equilibrium thrust is $F^* = mr_d\Omega^2$ with corresponding heading $\phi^* = 0$. Linearizing the system at this equilibrium point gives the linearized dynamics

$$\begin{bmatrix} \dot{x} \\ \dot{y} \\ \dot{v}_x \\ \dot{v}_y \\ \dot{\phi} \\ \dot{\omega} \end{bmatrix} = \begin{bmatrix} 0 & 0 & 1 & 0 & 0 & 0 \\ 0 & 0 & 0 & 1 & 0 & 0 \\ \Omega^2 & 0 & 0 & 2\Omega & r_d\Omega^2 & 0 \\ 0 & \Omega^2 & -2\Omega & 0 & 0 & 0 \\ 0 & 0 & 0 & 0 & 0 & 1 \\ 0 & 0 & 0 & 0 & 0 & 0 \end{bmatrix} \begin{bmatrix} x \\ y \\ v_x \\ v_y \\ \phi \\ \omega \end{bmatrix} + \begin{bmatrix} 0 & 0 \\ 0 & 0 \\ 0 & 0 \\ -\frac{1}{m} & 0 \\ 0 & 0 \\ 0 & \frac{1}{I} \end{bmatrix} \begin{bmatrix} F \\ \tau \end{bmatrix} \quad (16)$$

The controllability matrix for this new system, $M_{c,r}$, is given by

$$M_{c,r} = \begin{bmatrix} 0 & 0 & 0 & 0 & -\frac{2\Omega}{m} & 0 \\ 0 & 0 & -\frac{1}{m} & 0 & 0 & 0 \\ 0 & 0 & -\frac{2\Omega}{m} & 0 & 0 & \frac{r_d\Omega^2}{I} \\ -\frac{1}{m} & 0 & 0 & 0 & \frac{3\Omega^2}{m} & 0 \\ 0 & 0 & 0 & \frac{1}{I} & 0 & 0 \\ 0 & \frac{1}{I} & 0 & 0 & 0 & 0 \end{bmatrix} \quad \begin{matrix} \text{dependent} \\ \text{columns} \end{matrix} \quad (17)$$

The first six columns of this new controllability matrix are independent, meaning that the controllability matrix is full rank and that the system is controllable. Therefore, linear control techniques can be applied in order to regulate the spacecraft's position to the equilibrium state in the rotating frame. While this analysis was conducted in two dimensions, for clarity in the equations, the same results will occur in three dimensions. The spacecraft will be uncontrollable at the equilibrium state of the inertial frame but is controllable at the equilibrium state of the rotating frame.

III. Baseline Orbit

The proposed baseline motion of the spacecraft during proximity operations is the circular orbit shown in Figure 2. As discussed in Section II, this orbit allows linear control methods to be applied to regulate the spacecraft's position and allow it to reject external disturbances. This orbit also has the bonus of implicitly avoiding plume impingements on the target. Since the spacecraft has to

thrust inwards, towards the target, in order to provide the necessary centripetal acceleration, the plume of the propulsion system will be directed away from the target. In addition, the side of the spacecraft opposite from the propulsion system will always be pointed towards the target, providing a convenient location for cameras for visual inspection or other scientific instruments.

While the circular orbit allows for linear position control and avoids plume impingement, it does require a constant acceleration to be provided by the propulsion system, creating two potential downsides to this strategy. First, the propulsion system needs to be able to produce the necessary centripetal thrust. This is indirectly a constraint on the overall time for the mission as the required thrust can be made arbitrarily small by decreasing the orbital frequency, at the cost of slower maneuvers. Second, even in a scenario with zero external disturbances, the spacecraft will constantly be using propellant. However, the low required centripetal acceleration and high efficiency of electrospray propulsion means that this propellant cost is negligible.

As an example scenario, consider a 3U CubeSat inspector spacecraft with mass of 4 kg and an electrospray thruster propulsion system capable of producing a thrust of 250 μN . If the desired inspection radius is 25 m, then the maximum orbit frequency that can be maintained is

$$\Omega_{\max} = \sqrt{\frac{F}{mr}} \quad (18)$$

and is 1.6 mrad/s. The period of the inspection orbit is therefore 66 minutes, which is still faster than the 90 minute inspection period that would be allowed by natural orbital dynamics in low-Earth orbit. Assuming the propellant mass is negligible relative to the overall mass of the spacecraft, the required propellant per orbit can be approximated from

$$m_f = \frac{F}{I_{\text{sp}}g} \frac{2\pi}{\Omega_{\max}} = \frac{2\pi\sqrt{Fmr}}{I_{\text{sp}}g} \quad (19)$$

where I_{sp} is the specific impulse of the propulsion system and g is the standard gravitational acceleration. Typical specific impulses for electrospray thrusters are on the order of 1000 s. In this scenario, the spacecraft will use 101 mg of propellant per orbit and could perform almost 10 inspection orbits before using a gram of fuel. Comparatively, for a cold-gas propulsion system with a specific impulse of 80 s, the propellant used per orbit is 1.3 g and would allow for almost 0.8 orbits per gram of fuel.

IV. Maneuver Library

In order to make use of the baseline orbit, several maneuvers need to be designed. Most importantly, the spacecraft needs to be able to join the circular orbit from a stationary position as well as leave the circular orbit to a stationary position. Both joining and leaving the circular orbit are the same process just executed in opposite directions in time, and therefore will be considered a single maneuver. Next, the spacecraft needs to be able to change the radius of the circular orbit. With these two maneuvers, joining/leaving the circular orbit and changing the orbit's radius, the spacecraft will be able to perform point-to-point maneuvering through a series of waypoints in three dimensions, circumnavigation maneuvers, as well as landing or docking to a rotating target.

The remaining maneuvers do not add additional functionality but simplify the overall mission design. Changing the frequency of the orbit could be accomplished by leaving the initial orbit and then joining a new orbit of the desired new frequency. However, it is relatively simple to design maneuvers to increase or decrease the orbit frequency within the framework developed here. Similarly, translating the orbital plane along its normal vector could be achieved by a convoluted set of maneuvers, but it is relatively simple to design a single maneuver to accomplish this task.

All maneuvers are designed by leveraging the differential flatness of the underactuated spacecraft. In particular, by defining the input thrust within the orbital plane as well as constraining that the spacecraft either maintain a constant radius or constant orbital frequency, the entire state of the spacecraft can be determined including the spacecraft's heading and rotational velocity with respect to the rotating frame. It is assumed that the coordinate frame is always defined such that the x and y axes lie in the maneuver plane and that the frequency of the rotating frame, Ω , is along the positive z direction.

For dynamic consistency, any maneuvers that begin or end on the circular trajectory need to have a nadir-pointing attitude such that there are no discontinuities between the spacecraft's heading at the boundaries of the maneuver and the circular orbit. In addition, the rotational velocity of the spacecraft with respect to the rotating frame needs to be zero at the beginning and end of all maneuvers. Figure 3 shows the spacecraft in the rotating frame with the heading of the spacecraft, ϕ , defined as anticlockwise rotation relative to a nadir-pointing attitude. For maneuver design, it

is assumed that the spacecraft is on the positive y -axis of the rotating frame such that $x = 0$ and $y > 0$ and that the magnitude of the frequency of the rotating frame, Ω , is modulated in order to maintain $x = 0$. The dynamics in the rotating frame for a variable frequency are

$$\vec{a}_i(t) = \vec{a}_r(t) + 2\vec{\Omega}(t) \times \vec{v}_r(t) + \dot{\vec{\Omega}}(t) \times \vec{r}_r(t) + \vec{\Omega}(t) \times (\vec{\Omega}(t) \times \vec{r}_r(t)) \quad (20)$$

Assuming that $\vec{\Omega}$ still points purely in the \hat{z} direction with magnitude Ω , then the dynamics in the x - y plane are

$$\ddot{x}(t) = \Omega^2(t)x(t) + 2\Omega(t)\dot{y}(t) + \dot{\Omega}(t)y(t) + a_x(t) \quad (21)$$

$$\ddot{y}(t) = \Omega^2(t)y(t) - 2\Omega(t)\dot{x}(t) - \dot{\Omega}(t)x(t) + a_y(t) \quad (22)$$

Under the condition that $x = 0$ for all time, then the dynamics become

$$0 = 2\Omega(t)\dot{y}(t) + \dot{\Omega}(t)y(t) + a_x(t) \quad (23)$$

$$\ddot{y}(t) = \Omega^2(t)y(t) + a_y(t) \quad (24)$$

Given a particular input acceleration of a_x along the x -axis and a_y along the y -axis, the heading of the spacecraft can be calculated from

$$\tan \phi(t) = -\frac{a_x(t)}{a_y(t)} \quad (25)$$

In situations in which the spacecraft needs to have a nadir-pointing attitude this confirms the intuition that $a_x = 0$ and $a_y < 0$, or that the spacecraft is producing an acceleration towards the center of the circular orbit. The spacecraft's rotational velocity, ω , can be calculated by taking the time derivative of both sides of Eq. 25 and solving for ω as

$$\omega(t) = \frac{1}{a_x^2(t) + a_y^2(t)} \left(a_x(t) \frac{d}{dt} a_y(t) - a_y(t) \frac{d}{dt} a_x(t) \right) \quad (26)$$

Therefore, in order to ensure that $\omega = 0$ at the beginning and end of each maneuver the constraints

$$a_x(t) = 0 \quad \text{or} \quad \frac{d}{dt} a_y(t) = 0 \quad (27)$$

and

$$a_y(t) = 0 \quad \text{or} \quad \frac{d}{dt} a_x(t) = 0 \quad (28)$$

need to be satisfied at the beginning and end of each maneuver.

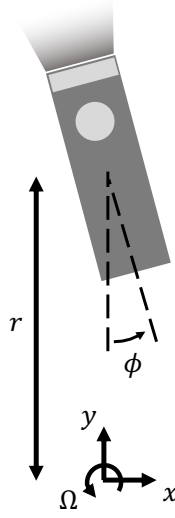


Fig. 3 Spacecraft in the rotating frame.

A. Joining Orbit from Rest

The goal of the joining-orbit maneuver is to transition the spacecraft from a static position to a circular orbit around the target of desired radius r_d and frequency Ω_d . Since the spacecraft does not start this maneuver on the circular orbit, it is not required to have a nadir-pointing attitude at the start of the maneuver and can start in any desired attitude.

The approach for designing the joining-orbit maneuver is to constrain the radial position of the spacecraft to be constant at the desired radial position, r_d . Under this condition, the dynamics from Eqs. 23 and 24 become

$$0 = \dot{\Omega}(t)r_d + a_x(t) \quad (29)$$

$$0 = \Omega^2(t)r_d + a_y(t) \quad (30)$$

$\Omega(t)$ is then driven from zero to the desired frequency, Ω_d , by selecting the correct profile for $a_x(t)$.

After solving for $\Omega(t)$, $a_y(t)$ can then be solved for from Eq. 30

Consider a polynomial profile for a_x of the form

$$a_x(t) = -a_1 \left(1 - \frac{t}{t_{p,1}}\right)^n \quad (31)$$

where a_1 is a positive constant, $t_{p,1}$ is the overall time of the maneuver, and n is a free parameter that sets the degree of the profile. By design, $a_x(t_{p,1}) = 0$ and $\dot{a}_x(t_{p,1}) = 0$ as long as $n > 1$.

Therefore, the rotational velocity of the spacecraft in the rotating frame will be zero at the end of the trajectory. In addition, since $a_x(t_{p,1}) = 0$ and $a_y(t_{p,1}) = -r_d\Omega_d^2$, the spacecraft will have a nadir-pointing attitude at the end of the trajectory.

The frequency of the orbit can be solved for as

$$\Omega(t) = -\frac{1}{r_d} \int_0^t a_x(\tau) d\tau \quad (32)$$

$$= \frac{a_1 t_{p,1}}{(n+1)r_d} \left[1 - \left(1 - \frac{t}{t_{p,1}} \right)^{n+1} \right] \quad (33)$$

which, based on Eq. 30, gives the thrust along the y -axis of

$$a_y(t) = -\frac{a_1^2 t_{p,1}^2}{(n+1)^2 r_d} \left[1 - \left(1 - \frac{t}{t_{p,1}} \right)^{n+1} \right]^2 \quad (34)$$

At the beginning of the trajectory $a_y(0) = 0$ and $\dot{a}_y(0) = 0$ which means that the rotational velocity of the spacecraft will be zero at the beginning of the trajectory.

The trajectory needs to be correctly sized, by setting a_1 and $t_{p,1}$, such that $\Omega(t_{p,1}) = \Omega_d$. Since

$$\Omega(t_{p,1}) = \frac{a_1 t_{p,1}}{(n+1)r_d} \quad (35)$$

then the choice of a_1 and $t_{p,1}$ must satisfy

$$a_1 t_{p,1} = (n+1)r_d \Omega_d \quad (36)$$

An additional constraint could be that the required acceleration does not exceed the maximum acceleration output of the propulsion system

$$a^2(t) = a_x^2(t) + a_y^2(t) \leq \left(\frac{F_{\max}}{m} \right)^2 \quad \forall t \in [0, t_{p,1}] \quad (37)$$

On the range $0 < t < t_{p,1}$ there are no local maxima for the magnitude of the required acceleration, the proof for which is shown in Appendix A. Since there are no local maxima on the range $0 < t < t_{p,1}$, then the maximum acceleration of the profile occurs on the boundary: either $t = 0$ or $t = t_{p,1}$.

The maximum acceleration is therefore

$$\max \left(\sqrt{a^2(t)} \right) = a_1 \quad \text{or} \quad \max \left(\sqrt{a^2(t)} \right) = r_d \Omega_d^2 \quad (38)$$

By design, it has to be that

$$r_d \Omega_d^2 \leq \frac{F_{\max}}{m} \quad (39)$$

otherwise the spacecraft would not be able to maintain the circular orbit. Therefore, the trajectory can be correctly sized by setting

$$a_1 = \frac{F_{\max}}{m} \quad (40)$$

Combining Eq. 40 with Eq. 36, then the total time of the maneuver is also set as

$$t_{p,1} = \frac{(n+1)r_d\Omega_d}{F_{\max}/m} \quad (41)$$

The remaining state to be solved for is the angular position of the spacecraft over time. The change in angular position is

$$\Delta\theta(t) = \int_0^t \Omega(\tau) d\tau \quad (42)$$

$$= -\frac{a_1 t_{p,1}^2}{(n+1)r} \left(\frac{1}{n+2} \left[1 - \left(1 - \frac{t}{t_{p,1}} \right)^{n+2} \right] - \frac{t}{t_{p,1}} \right) \quad (43)$$

which gives a total angular change of the spacecraft over the course of the maneuver of

$$\Delta\theta(t_{p,1}) = \frac{a_1 t_{p,1}^2}{(n+2)r} = \frac{(n+1)^2}{n+2} \frac{r_d \Omega_d^2}{F_{\max}/m} \quad (44)$$

B. Changing Orbital Radius

Once the spacecraft is on the desired circular orbit, it needs to be able to change the radius of the circular orbit in order to enable point-to-point maneuvering. The ability to change the orbit's radius could also be used to land on or dock to a rotating target by slowing lowering the orbit's radius.

The maneuver can be designed starting from the dynamics given by Eqs. 23 and 24 and assuming that the frequency of the rotating frame is held constant at Ω_d throughout the maneuver. This results in the dynamics

$$0 = 2\Omega_d \dot{y}(t) + a_x(t) \quad (45)$$

$$\ddot{y}(t) = \Omega_d^2 y(t) + a_y(t) \quad (46)$$

For this maneuver, the strategy is to pick $a_y(t)$ in order to drive $y(t)$, the radius of the orbit, from the initial radius to the desired radius. Once $y(t)$ has been solved for, the required profile for $a_x(t)$

can be solved for from Eq. 45, which will hold the frequency of the orbit constant throughout the maneuver.

Consider a profile for $a_y(t)$ of the form

$$a_y(t) = -\Omega_d^2 y(t) + a_2 t(t - t_{p,2})(t - 0.5t_{p,2}) \quad (47)$$

where a_2 is a constant and $t_{p,2}$ is the overall time of the maneuver. With this profile, the radial dynamics become

$$\ddot{y}(t) = a_2 t(t - t_{p,2})(t - 0.5t_{p,2}) \quad (48)$$

which results in a radial velocity of

$$\dot{y}(t) = \int_0^t \ddot{y}(\tau) d\tau \quad (49)$$

$$= \frac{1}{4} a_2 t^2 (t - t_{p,2})^2 \quad (50)$$

and overall change in radius of

$$\Delta y(t) = \int_0^t \dot{y}(\tau) d\tau \quad (51)$$

$$= \frac{1}{120} a_2 t^3 (6t^2 - 15t_{p,2}t + 10t_{p,2}^2) \quad (52)$$

The change in radius over the course of the entire maneuver is

$$\Delta y(t_{p,2}) = \frac{1}{120} a_2 t_{p,2}^5 \quad (53)$$

Therefore, for a desired change in radius, Δr , the parameters a_2 and $t_{p,2}$ need to be set such that

$$a_2 t_{p,2}^5 = 120 \Delta r \quad (54)$$

The thrust profile along each axis is then

$$a_x(t) = -2\Omega_d \dot{y}(t) \quad (55)$$

$$= -\frac{1}{2} a_2 \Omega_d t^2 (t - t_{p,2})^2 \quad (56)$$

and

$$a_y(t) = -\Omega_d^2 (y_0 + \Delta y(t)) + a_2 t(t - t_{p,2})(t - 0.5t_{p,2}) \quad (57)$$

$$= -\Omega_d^2 \left[y_0 + \frac{a_2}{120} t^3 (6t^2 - 15t_{p,2}t + 10t_{p,2}^2) \right] + a_2 t(t - t_{p,2})(t - 0.5t_{p,2}) \quad (58)$$

where y_0 is the initial orbital radius. As with the joining-orbit maneuver, the thrust profile should be further constrained such that the maximum thrust required for the profile is less than the maximum thrust of the propulsion system. This would amount to finding the critical points of the overall thrust magnitude by solving

$$\frac{d}{dt} (a_x(t)^2 + a_y(t)^2) = 0 \quad (59)$$

To the authors' knowledge, these critical points cannot be solved for analytically. Therefore, an alternative approach to bounding the required thrust is used. The maximum magnitude of the thrust along the x axis is

$$\max_{t \in [0, t_{p,2}]} \left(\left| -\frac{1}{2} a_2 \Omega_d t^2 (t - t_{p,2})^2 \right| \right) = \frac{1}{32} \Omega_d |a_2| t_{p,2}^4 \quad (60)$$

The thrust along the y -axis can be broken into two components. The first is the centripetal force which has a maximum magnitude of

$$\max_{t \in [0, t_{p,2}]} |a_{y,\text{centripetal}}| = \Omega_d^2 \max(y_0, y_0 + \Delta r) \quad (61)$$

The second component is the cubic function added on-top of the centripetal force in order to change the orbit's radius. This component has a maximum magnitude of

$$\max_{t \in [0, t_{p,2}]} |a_2 t (t - t_{p,2}) (t - 0.5 t_{p,2})| = \frac{1}{12\sqrt{3}} |a_2| t_{p,2}^3 \quad (62)$$

Therefore, the magnitude of the thrust vector is bounded by

$$\sqrt{a_x^2(t) + a_y^2(t)} \leq \frac{1}{32} \Omega_d |a_2| t_{p,2}^4 + \Omega_d^2 \max(y_0, y_0 + \Delta r) + \frac{1}{12\sqrt{3}} |a_2| t_{p,2}^3 \quad (63)$$

which means that by setting

$$\frac{1}{32} \Omega_d |a_2| t_{p,2}^4 + \Omega_d^2 \max(y_0, y_0 + \Delta r) + \frac{1}{12\sqrt{3}} |a_2| t_{p,2}^3 = \frac{F_{\max}}{m} \quad (64)$$

the maximum thrust required for the maneuver will be guaranteed to be lower than the maximum thrust of the propulsion system. From Eq. 54 it must be that

$$|a_2| = \frac{120 |\Delta r|}{t_{p,2}^5} \quad (65)$$

which when substituted into Eq. 64 gives a profile time of

$$t_{p,2} = \frac{\frac{15}{4}\Omega_d|\Delta r| + \sqrt{\frac{225}{16}\Omega_d^2\Delta r^2 + \frac{40}{\sqrt{3}}(F_{\max}/m - \Omega_d^2 \max(y_0, y_0 + \Delta r))}|\Delta r|}{2(F_{\max}/m - \Omega_d^2 \max(y_0, y_0 + \Delta r))} \quad (66)$$

While this profile time does guarantee that the maximum acceleration required will be within the capabilities of the propulsion system, it is possible for $a_y(t) > 0$ during some parts of the maneuver which means that the plume of the propulsion system starts to point radially inwards, towards the target. The fact that $a_y(t) > 0$ for some range of the maneuver does not necessarily mean that plume impingement will occur, but without any bound on the value of $a_y(t)$ it cannot be guaranteed that plume impingement will be avoided. For this reason, it is worth developing an alternative setting of the parameters a_2 and $t_{p,2}$ in order to bound $a_y(t)$. The most convenient bound is to ensure that $a_y(t) \leq 0$ for the entire maneuver and develop guarantees for avoiding plume impingement based on this constraint, which will be covered in Section V. Such a bound will also match the characteristics of the joining-orbit maneuver where $a_y(t) \leq 0$ for the entire maneuver.

A simple way to bound $a_y(t) \leq 0$ is to ensure that the maximum magnitude of the cubic portion of $a_y(t)$ does not exceed the minimum value of the centripetal acceleration

$$\max_{t \in [0, t_{p,2}]} |a_2 t(t - t_{p,2})(t - 0.5t_{p,2})| \leq \min_{t \in [0, t_{p,2}]} |a_{y,\text{centripetal}}| \quad (67)$$

which can be ensured by solving

$$\frac{1}{12\sqrt{3}}|a_2|t_{p,2}^3 \leq \Omega_d^2 \min(y_0, y_0 + \Delta r) \quad (68)$$

Solving for the resulting profile time gives

$$t_{p,2} = \sqrt{\frac{10|\Delta r|}{\sqrt{3}\Omega_d^2 \min(y_0, y_0 + \Delta r)}} \quad (69)$$

Given the two possible bounds for the profile time from Eqs. 66 and 69, the larger of the two possible profile times is selected for a given scenario. This ensures both that the maximum thrust of the propulsion system will not be exceeded and that the radial acceleration will always be negative. In most cases Eq. 69 will constrain the profile time, however in cases where

$$F_{\max}/m \approx \Omega_d^2 \max(y_0, y_0 + \Delta r) \quad (70)$$

then Eq. 66 will be the applicable constraint.

C. Changing Orbital Frequency

Changing the orbit's frequency is similar to joining the orbit from rest, only that the spacecraft initially starts on a circular orbit. Starting from the dynamics given by Eqs. 29 and 30 then the goal is to pick a profile for $a_x(t)$ to drive the frequency of the orbit from some initial frequency, Ω_0 to a desired frequency Ω_d while maintaining a constant radius of r_d . Since the spacecraft starts and ends on a circular orbit, the profile needs to satisfy $a_x(0) = a_x(t_p) = 0$. In addition, $a_y(0) = -r_d\Omega_0^2$ and $a_y(t_p) = -r_d\Omega_d^2$ which means that for the spacecraft to have zero rotational velocity at the beginning and end of the trajectory, it must be that $\dot{a}_x(0) = \dot{a}_x(t_p) = 0$. All of this can be accomplished with a quartic polynomial

$$a_x(t) = -a_3 t^2 (t - t_{p,3})^2 \quad (71)$$

where a_3 is a constant and $t_{p,3}$ is the overall length of the maneuver.

With this profile for $a_x(t)$, the change in orbital frequency is given by

$$\Delta\Omega(t) = -\frac{1}{r_d} \int_0^t a_x(\tau) d\tau \quad (72)$$

$$= \frac{a_3 t^3}{30r_d} (6t^2 - 15tt_{p,3} + 10t_{p,3}^2) \quad (73)$$

with a total change in orbital frequency over the entire maneuver of

$$\Delta\Omega(t_{p,3}) = \frac{1}{30} \frac{a_3 t_{p,3}^5}{r_d} \quad (74)$$

Therefore, for a given initial frequency of Ω_0 and final frequency of Ω_d , the parameters a_3 and $t_{p,3}$ must be selected in order to satisfy

$$a_3 t_{p,3}^5 = 30r_d(\Omega_d - \Omega_0) \quad (75)$$

The profile for $a_y(t)$ can then be solved for from Eq. 30 as

$$a_y(t) = -r_d \left[\Omega_0 + \frac{a_3 t^3}{30r_d} (6t^2 - 15tt_{p,3} + 10t_{p,3}^2) \right]^2 \quad (76)$$

As with the orbital radius change, an analytical expression for the critical points of the overall thrust magnitude could not be found. However, under the parameter settings

$$a_3 = \frac{9}{160} \frac{r_d (\Omega_d + \Omega_0)}{\Omega_d - \Omega_0} \left(\frac{1600}{3} \frac{(\Omega_d - \Omega_0)^2}{(\Omega_d + \Omega_0)^6} \right)^{-1/4} \quad (77)$$

and

$$t_{p,3} = \left(\frac{1600}{3} \frac{(\Omega_d - \Omega_0)^2}{(\Omega_d + \Omega_0)^6} \right)^{1/4} \quad (78)$$

it is guaranteed that the maximum acceleration magnitude occurs either at $t = 0$ or $t = t_{p,3}$, the proof for which is shown in Appendix B. Since the maximum occurs on the boundaries of the trajectory, the maximum acceleration magnitude is

$$\max_{t \in [0, t_{p,3}]} a(t) = r_d \max(\Omega_0^2, \Omega_d^2) \quad (79)$$

Finally, the angular position of the spacecraft throughout the maneuver is given by

$$\Delta\theta(t) = \int_0^t \Omega(\tau) d\tau \quad (80)$$

$$= \Omega_0 t_{p,3} + \frac{1}{60} \frac{a_3 t^4}{r_d} (2t^2 - 6t_{p,3}t + 5t_{p,3}^2) \quad (81)$$

which gives an overall angular change of the spacecraft from the maneuver of

$$\Delta\theta(t_{p,3}) = \frac{t_{p,3}}{2} (\Omega_0 + \Omega_d) \quad (82)$$

D. Changing Orbital Plane

Changing the orbital plane could have two different goals. The first would be to rotate the orbital plane around some axis, analogous to an inclination change in orbital dynamics. The second is to translate the orbital plane along its normal vector. Rotating the orbital plane is most-easily accomplished by leaving the current circular orbit at the intersection point between the current orbital plane and desired orbital plane (the ascending or descending node) and then joining a new circular orbit in the desired orbital plane. Translating the orbital plane cannot be accomplished as easily and requires a separate maneuver.

Conveniently, in the chosen coordinate system the z -axis dynamics are decoupled from the in-plane dynamics

$$\ddot{z}(t) = a_z(t) \quad (83)$$

In order to ensure that the spacecraft's heading and rotational velocity are continuous between maneuvers, it must be that $a_z(0) = a_z(t_p) = 0$, $\dot{a}_z(0) = \dot{a}_z(t_p) = 0$, and $\dot{z}(0) = \dot{z}(t_p) = 0$. For

the maneuver, the goal is to translate the orbit through a height change of Δz_d . All of this can be accomplished with a quintic acceleration profile

$$a_z(t) = -a_4 t^2 (t - t_{p,4})^2 (t - 0.5t_{p,4}) \quad (84)$$

where a_4 is a constant and $t_{p,4}$ is the overall length of the maneuver.

This acceleration profile results in a z velocity of

$$\dot{z}(t) = \int_0^t a_z(\tau) d\tau \quad (85)$$

$$= -\frac{1}{6} a_4 t^3 (t^3 - 3t_{p,4} t^2 + 3t_{p,4}^2 t - t_{p,4}^3) \quad (86)$$

and a change in z position of

$$\Delta z(t) = \int_0^t \dot{z}(\tau) d\tau \quad (87)$$

$$= -\frac{1}{840} a_4 t^4 (20t^3 - 70t_{p,4} t^2 + 84t_{p,4}^2 t - 35t_{p,4}^3) \quad (88)$$

The parameters a_4 and $t_{p,4}$ need to be selected such that $\Delta z(t_{p,4}) = \Delta z_d$

$$\Delta z(t_{p,4}) = \frac{1}{840} a_4 t_{p,4}^7 \quad (89)$$

which places the requirement that

$$a_4 t_{p,4}^7 = 840 \Delta z_d \quad (90)$$

The maximum required acceleration can be analytically solved for. The maximum magnitude of the z acceleration is

$$\max_{t \in [0, t_{p,4}]} |a_z(t)| = \frac{1}{50\sqrt{5}} a_4 t_{p,4}^5 \quad (91)$$

while the acceleration in the x - y plane is held constant at $r_d \Omega_d^2$. Therefore, the trajectory can be correctly sized by solving

$$r_d^2 \Omega_d^4 + \frac{1}{12500} a_4^2 t_{p,4}^{10} = \left(\frac{F_{\max}}{m} \right)^2 \quad (92)$$

which results in a profile time of

$$t_{p,4} = \sqrt{\frac{84}{5\sqrt{5}}} \left(\frac{\Delta z_d^2}{(F_{\max}/m)^2 - r_d^2 \Omega_d^4} \right)^{1/4} \quad (93)$$

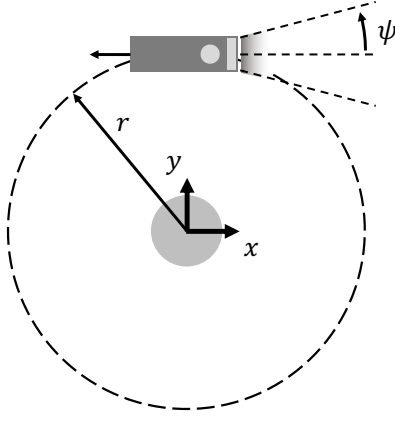


Fig. 4 Worst-case scenario for plume impingement where radial component of acceleration is zero.

V. Plume Impingement

All maneuvers were designed such that the radial component of the thrust vector is never positive. This allows for guarantees regarding plume impingement to be developed. In the worst-case scenario, the radial component of the thrust vector is zero, as it is at the very beginning of the joining-orbit maneuver. Figure 4 shows this scenario for a propulsion system plume half-angle of ψ . Assuming that it is desired for the plume to never intersect a sphere of radius R around the target, then limits on the minimum radius that the spacecraft is allowed to operate in can be developed. This minimum radius can be solved for from geometry as

$$r_{\min} = \frac{R}{\cos \psi} \quad (94)$$

As long as the desired baseline circular orbit of the spacecraft has a radius of $r > r_{\min}$ and the sphere of radius R is appropriately selected in order to fully encompass the target (such as a circumscribing sphere), plume impingement will be avoided.

VI. Examples

This section shows examples of the analytical maneuver library being used for basic mission segments. Specifically, point-to-point maneuvering between any two points in space is shown including situations where the central target is cylindrical and changing the orbit height may be advantageous. In addition, the use of changing the orbit frequency and changing orbit radius is demonstrated for

landing or docking to a rotating target.

In all cases, the construction of the full maneuver from individual maneuvers in the library is the same. First, the necessary maneuvers are selected including the addition of a “coast” maneuver where the spacecraft simply maintains its current circular orbit. The maneuvers are then stitched together at their boundaries in order to form a full maneuver and the “coast” maneuver is used in order to fill in any necessary gaps in angular position. Since all maneuvers, with the exception of joining or leaving the circular orbit, were designed to start and end at the same attitude (nadir pointing attitude with zero rotational velocity), stitching different maneuvers from the library together is as simple as ensuring that they have the same radial and angular position within the desired orbital plane.

A. Point-to-Point

Figure 5 shows an example of point-to-point maneuvering between two waypoints. The full maneuver is composed of joining the circular orbit, coasting, changing the orbital radius, and finally leaving the circular orbit. The ordering of coasting and changing orbital radius can change depending on if the end waypoint is at a greater or lower radius than the start waypoint. The acceleration required to maintain a circular orbit of a given frequency increases with orbit radius, so coasting usually should occur at as low of an orbital radius as possible. In the scenario in Figure 5 since the end waypoint is at a greater radius than the start waypoint, coasting is conducted before increasing the orbit radius.

Figure 6 shows the spacecraft’s heading and rotational velocity in the rotating frame throughout the full maneuver. At the boundaries between individual maneuvers, the spacecraft always returns to a nadir-pointing attitude with zero rotational velocity which makes stitching together the individual maneuvers quite simple. In addition, the spacecraft’s heading in the rotating frame always remains between $\pm 90^\circ$ which means that the spacecraft’s thrust vector never points radially inwards.

Since the spacecraft’s heading in the rotating frame remains between $\pm 90^\circ$, the conditions under which plume impingement is guaranteed to be avoided can be determined based on Eq. 94. The lowest radius of the spacecraft is 10 m, the radius of the start waypoint, which means that for

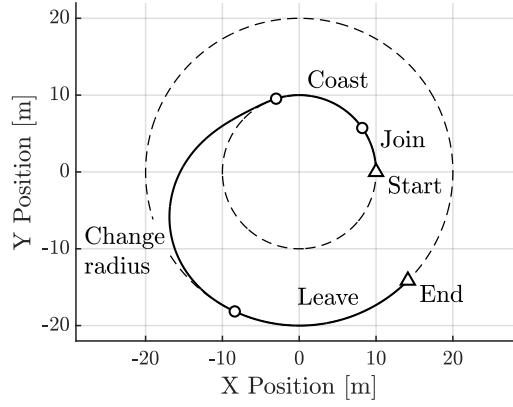


Fig. 5 Basic point-to-point maneuver.

an assumed plume half angle of 45° , Eq. 94 gives that the plume will never enter a sphere of radius 7.07 m. Figure 7 shows a plume impingement map for the maneuver. Regions on the map that would experience plume impingement at any point during the maneuver are shaded. Darker shading corresponds to regions that would experience plume impingement for a greater duration of time while regions that are unshaded would not experience plume impingement at any point during the maneuver. Since the thrust vector of the spacecraft propulsion system predominantly points towards the center, in order to produce an inward-pointing centripetal force, most of the shading is on regions that are radially outward from the spacecraft trajectory. A circle of radius 7.07 m is marked on the plot, and it can be seen that the plume of the spacecraft does not enter this circle.

B. Cylindrical Point-to-Point

For cylindrical targets, such as the upper-stage of a booster, the use of the changing-height maneuver might be advantageous. Although passively-safe trajectories are not explicitly addressed in this work, around a more spherical target if the propulsion system of the spacecraft happens to fail while the spacecraft is maintaining its circular orbit, the spacecraft will drift away from the target with no risk of collision. Around a cylindrical target, if the normal vector of the orbit is not parallel to the long axis of the target it is possible for the orbit to intersect the target. For this reason, it may be better to maintain circular orbits with their normal vector parallel to the long axis of the target, and use the changing-height maneuver to move along the target.

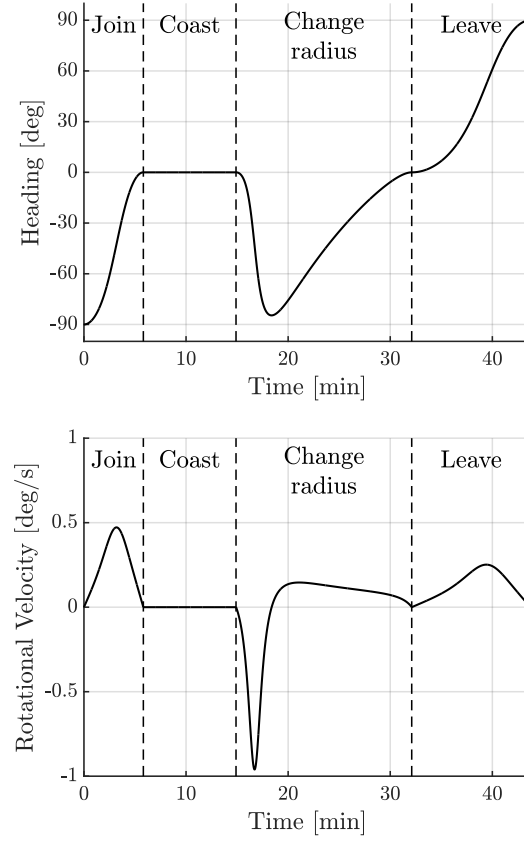


Fig. 6 Heading and rotational velocity of the spacecraft in the rotating frame throughout a basic point-to-point maneuver.

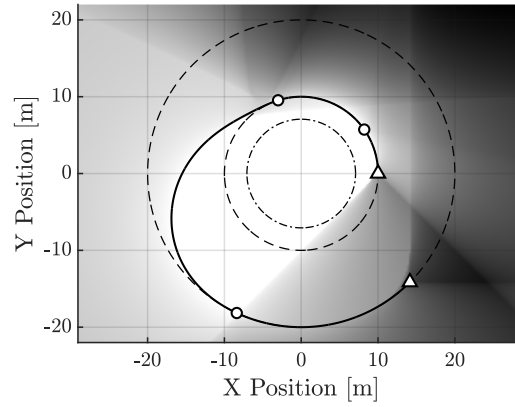


Fig. 7 Plume impingement map throughout a basic point-to-point maneuver. Shaded regions experience plume impingement with darker regions corresponding to greater plume impingement.

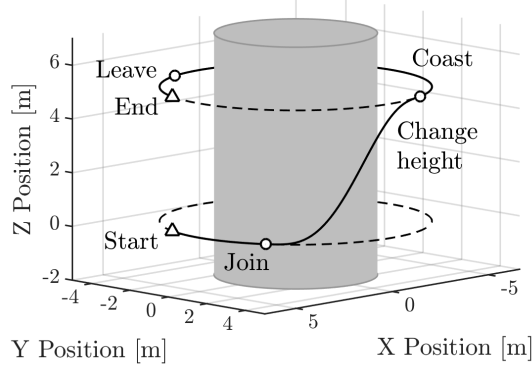


Fig. 8 Point-to-point maneuvering around a cylindrical target.

Figure 8 demonstrates one such application. Although it is possible to connect the start and end waypoints with a circular trajectory, the circle will end up intersecting the target, posing a potential collision risk. By using the changing-height maneuver, the spacecraft can move from the start waypoint to the end waypoint on an entirely passively-safe trajectory - if the propulsion system of the spacecraft were to fail at any point of the trajectory, the spacecraft would drift away from the target with no risk of collision.

C. Landing/Docking

The changing orbital frequency and changing orbital radius maneuvers can be used to land on or dock to a rotating target. Figure 9 shows an example trajectory both in the inertial frame and in a frame rotating with the target. It is assumed that the spacecraft starts in a circular orbit with frequency equal to the rotational frequency of the target, such that in the rotating frame the spacecraft is stationary.

The spacecraft initially starts 30° behind its desired landing/docking point. Therefore, before landing it first must increase its own orbit frequency in order to catch up with the landing/docking point. This is conducted in three steps. First, the spacecraft increases its orbital frequency to some value larger than the targets rotational frequency. Next, the spacecraft coasts in order to allow itself to catch up with the desired landing/docking point. Finally, the spacecraft decreases its orbital frequency back down to the rotational frequency of the target such that it is hovering

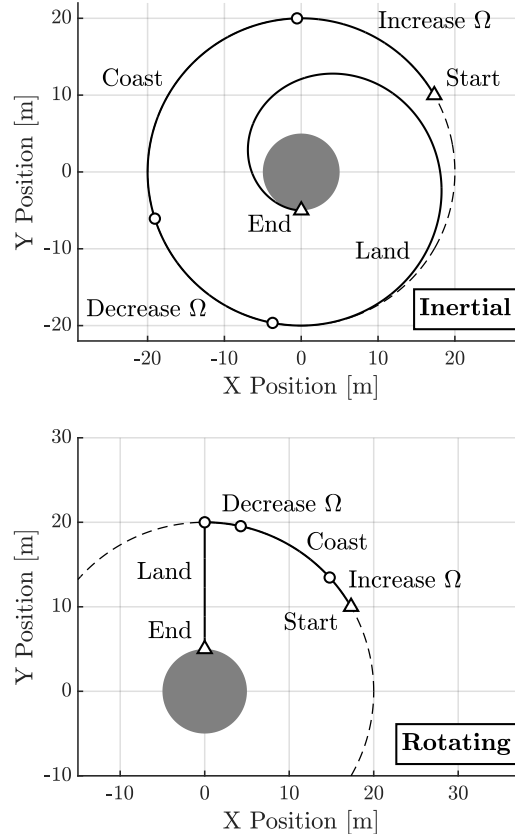


Fig. 9 Landing on or docking to a rotating target. The rotating frame rotates with the target which is assumed to be in a flat spin.

directly above the desired landing/docking point. At this point the spacecraft can lower its orbital radius such that it soft lands on/docks to the target. Since the maneuver for changing orbital radius was constrained to maintain a constant orbital frequency, the landing/docking maneuver appears as a straight line in the rotating frame.

Figure 10 shows a plume impingement map in the rotating frame throughout this maneuver. Since the spacecraft's final orbital radius is equal to the radius of the target, there are no guarantees regarding plume impingement unless the propulsion system's plume has zero width. However, by increasing the profile time beyond that specified by Eq. 69 plume impingement can still be avoided, as shown by Figure 10.

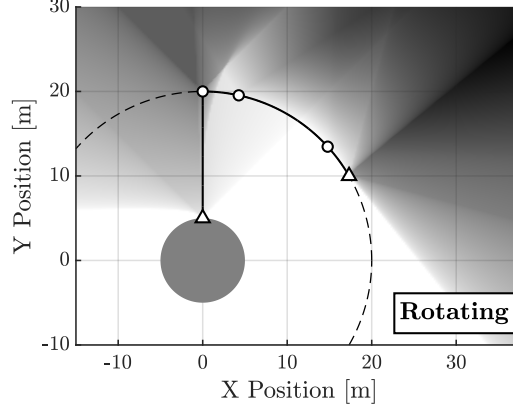


Fig. 10 Plume impingement map throughout landing on a rotating target. Shaded regions experience plume impingement with darker regions corresponding to greater plume impingement.

VII. Conclusion

This work demonstrates that an analytical maneuver library can be developed in order to maneuver an underactuated spacecraft around a central target without resorting to numerical optimization. Although the maneuver library developed in this work uses polynomial functions, other functions can be used such as trigonometric functions.

An analytical maneuver library could enable the use of high-efficiency but low-thrust propulsion systems, such as electrospray thrusters, for free-flying small spacecraft inspectors. Such spacecraft could be used for long-duration inspection of a target or a single spacecraft could be used to inspect multiple targets. While the maneuvers are suboptimal, the degree of suboptimality is marginal and trajectories can be computed at a significantly lower computational cost relative to methods that require numerical optimization.

Appendix A

The left side of Eq. 37 is

$$a^2(t) = a_1^2 \left(1 - \frac{t}{t_{p,1}}\right)^{2n} + \frac{a_1^4 t_{p,1}^4}{(n+1)^4 r_d^2} \left[1 - \left(1 - \frac{t}{t_{p,1}}\right)^{n+1}\right]^4 \quad (95)$$

To find its maximum, its critical points on the range $0 \leq t \leq t_{p,1}$ need to be solved for from

$$\frac{d}{dt} a^2(t) = 0 \quad (96)$$

which gives

$$\begin{aligned} \frac{d}{dt}a^2(t) = & -\frac{2na_1^2}{t_{p,1}} \left(1 - \frac{t}{t_{p,1}}\right)^{2n-1} \\ & + \frac{4a_1^4 t_{p,1}^3}{(n+1)^3 r_d^2} \left(1 - \frac{t}{t_{p,1}}\right)^n \left[1 - \left(1 - \frac{t}{t_{p,1}}\right)^{n+1}\right]^3 \end{aligned} \quad (97)$$

Acknowledging that a critical point exists for $t = t_{p,1}$, then the remaining critical points can be found by solving

$$\left(1 - \frac{t}{t_{p,1}}\right)^{n-1} = \frac{2a_1^2 t_{p,1}^4}{n(n+1)^3 r_d^2} \left[1 - \left(1 - \frac{t}{t_{p,1}}\right)^{n+1}\right]^3 \quad (98)$$

Using the substitutions

$$u = 1 - \frac{t}{t_{p,1}} \quad \text{and} \quad A = \frac{2a_1^2 t_{p,1}^4}{n(n+1)^3 r_d^2} \quad (99)$$

then Eq. 98 can be written as

$$u^{n-1} = A [1 - u^{n+1}]^3 \quad (100)$$

There exists exactly one solution to this equation for the range $0 < u < 1$ since on this range the left-hand side is monotonically increasing from 0 to 1 and the right-hand side is monotonically decreasing from A to 0. Therefore, on the range $0 < t < t_{p,1}$ there is only a single critical point. Furthermore,

$$\frac{d}{dt}a^2(0) = -\frac{2na_1^2}{t_{p,1}} < 0 \quad (101)$$

which indicates that the critical point cannot be a maxima. If it were a maxima, then just before the critical point the thrust magnitude would be increasing, $\frac{d}{dt}a^2(0) > 0$. However, for this to be possible, a local minima must have occurred earlier on in the profile since the thrust magnitude is initially decreasing. If this were the case, then the maxima is at least the second critical point. Since there can only exist a single critical point, no local maxima can exist.

Appendix B

The square of the total acceleration magnitude given Eqs. 71 and 76 is

$$a^2(t) = a_x^2(t) + a_y^2(t) \quad (102)$$

$$= a_3^2 t^4 (t - t_{p,3})^4 + r_d^2 \left[\Omega_0 + \frac{a_3 t^3}{30 r_d} (6t^2 - 15tt_{p,3} + 10t_{p,3}^2) \right]^4 \quad (103)$$

taking its derivative, to solve for the critical points, gives

$$\begin{aligned} \frac{d}{dt}a^2(t) &= 4a_3^2t^3(t - t_{p,3})^4 + 4a_3^2t^4(t - t_{p,3})^3 \\ &\quad + 4a_3r_d t^2(t - t_{p,3})^2 \left[\Omega_0 + \frac{a_3 t^3}{30r_d} (6t^2 - 15tt_{p,3} + 10t_{p,3}^2) \right]^3 \end{aligned} \quad (104)$$

Acknowledging the two critical points at $t = 0$ and two further critical points at $t = t_{p,3}$, then the remaining critical points can be found by solving

$$a_3t(t - t_{p,3})(2t - t_{p,3}) = -r_d \left[\Omega_0 + \frac{a_3 t^3}{30r_d} (6t^2 - 15tt_{p,3} + 10t_{p,3}^2) \right]^3 \quad (105)$$

An analytical solution for the critical points could not be found. However, the right-hand side of Eq. 105 is simply $-r_d\Omega(t)^3$ which is bounded by $-r_d\Omega_0^3$ and $-r_d\Omega_d^3$ and the left-hand side is a cubic function with roots at $t = 0$, $t = 0.5t_{p,3}$, and $t = t_{p,3}$. The maximum magnitude of the left-hand side is

$$\max_{t \in [0, t_{p,3}]} |a_3t(t - t_{p,3})(2t - t_{p,3})| = \frac{1}{6\sqrt{3}}a_3t_{p,3}^3 \quad (106)$$

Additionally, note from Eq. 54 that when $\Omega_d > \Omega_0$ then $a_3 > 0$ and the left-hand side of Eq. 105 is positive for $t < 0.5t_{p,3}$. When $\Omega_d < \Omega_0$ then $a_3 < 0$ and the left-hand side of Eq. 105 is positive for $t > 0.5t_{p,3}$. What this means is that when the left-hand and right-hand sides of Eq. 105 are the same sign, the right-hand side must be less than $-r_d \left[\frac{1}{2}(\Omega_0 + \Omega_d) \right]^3$. Therefore, by ensuring that

$$\left| \frac{1}{6\sqrt{3}}a_3t_{p,3}^3 \right| < \left| \frac{1}{8}r_d(\Omega_0 + \Omega_d)^3 \right| \quad (107)$$

there cannot be any critical points on the range $0 < t < t_p$. Combining this result with Eq. 54 gives the parameter settings

$$a_3 = \frac{9}{160} \frac{r_d(\Omega_d + \Omega_0)}{\Omega_d - \Omega_0} \left(\frac{1600}{3} \frac{(\Omega_d - \Omega_0)^2}{(\Omega_d + \Omega_0)^6} \right)^{-1/4} \quad (108)$$

and

$$t_{p,3} = \left(\frac{1600}{3} \frac{(\Omega_d - \Omega_0)^2}{(\Omega_d + \Omega_0)^6} \right)^{1/4} \quad (109)$$

Funding Sources

Funding for this work was provided by the NASA Space Technology Mission Directorate through the Small Spacecraft Technology Program under grant 80NSSC18M0045 and through a NASA Space Technology Research Fellowship under grant 80NSSC18K1186. In addition, P. C. Lozano would like to thank the Miguel Alemán-Velasco Foundation for its support.

References

- [1] Walton, P., Cannon, J., Damitz, B., Downs, T., Glick, D., Holtom, J., Kohls, N., Laraway, A., Matheson, I., Redding, J., et al., “Passive CubeSats for Remote Inspection of Space Vehicles,” *Journal of Applied Remote Sensing*, Vol. 13, No. 3, doi:<https://doi.org/10.1117/1.JRS.13.032505>.
- [2] Pedrotty, S., Sullivan, J., Gambone, E., and Kirven, T., “Seeker Free-Flying Inspector GNC System Overview,” in “Proceedings of the 42nd AAS Guidance & Control Conference,” Breckenridge, CO, 2019.
- [3] Henshaw, C., Healy, L., and Roderick, S., “LIIVE: A Small, Low-Cost Autonomous Inspection Vehicle,” in “Proceedings of the AIAA Space Conference & Exposition,” Pasadena, CA, 2009, doi:<https://doi.org/10.2514/6.2009-6544>.
- [4] Fourie, D., Tweddle, B. E., Ulrich, S., and Saenz-Otero, A., “Flight Results of Vision-Based Navigation for Autonomous Spacecraft Inspection of Unknown Objects,” *Journal of Spacecraft and Rockets*, Vol. 51, No. 6, 2014, pp. 2016–2026, doi:<https://doi.org/10.2514/1.A32813>.
- [5] Kim, S. C., Shepperd, S. W., Norris, H. L., Goldberg, H. R., and Wallace, M. S., “Mission Design and Trajectory Analysis for Inspection of a Host Spacecraft by a Nicrosatellite,” in “Proceedings of the 28th IEEE Aerospace Conference,” IEEE, Big Sky, MT, 2007, doi:<https://doi.org/10.1109/AERO.2007.352811>.
- [6] Lemmer, K., “Propulsion for CubeSats,” *Acta Astronautica*, Vol. 134, 2017, pp. 231–243, doi:<https://doi.org/10.1016/j.actaastro.2017.01.048>.
- [7] Legge, R. S. and Lozano, P. C., “Electrospray Propulsion Based on Emitters Microfabricated in Porous Metals,” *Journal of Propulsion and Power*, Vol. 27, No. 2, 2011, pp. 485–495, doi:<https://doi.org/10.2514/1.50037>.
- [8] Krejci, D., Mier-Hicks, F., Thomas, R., Haag, T., and Lozano, P. C., “Emission Characteristics of Passively Fed Electrospray Microthrusters with Propellant Reservoirs,” *Journal of Spacecraft and Rockets*,

- Vol. 54, No. 2, 2017, pp. 447–458,
doi:<https://doi.org/10.2514/1.A33531>.
- [9] Grustan-Gutierrez, E. and Gamero-Castaño, M., “Microfabricated Electrospray Thruster Array with High Hydraulic Resistance Channels,” *Journal of Propulsion and Power*, Vol. 33, No. 4, 2017, pp. 984–991,
doi:<https://doi.org/10.2514/1.B36268>.
- [10] Mier-Hicks, F. and Lozano, P. C., “Electrospray Thrusters as Precise Attitude Control Actuators for Small Satellites,” *Journal of Guidance, Control, and Dynamics*, Vol. 40, No. 3, 2017, pp. 642–649,
doi:<https://doi.org/10.2514/1.G000736>.
- [11] Corpino, S. and Stesina, F., “Inspection of the Cis-Lunar Station Using Multi-Purpose Autonomous CubeSats,” *Acta Astronautica*, Vol. 175, 2020, pp. 591–605,
doi:<https://doi.org/10.1016/j.actaastro.2020.05.053>.
- [12] Kannenberg, K. C. and Boyd, I. D., “Three-Dimensional Monte Carlo Simulations of Plume Impingement,” *Journal of Thermophysics and Heat Transfer*, Vol. 13, No. 2, 1999, pp. 226–235,
doi:<https://doi.org/10.2514/2.6440>.
- [13] Tajmar, M., González, J., and Hilgers, A., “Modeling of Spacecraft-Environment Interactions on SMART-1,” *Journal of Spacecraft and Rockets*, Vol. 38, No. 3, 2001, pp. 393–399,
doi:<https://doi.org/10.2514/2.3697>.
- [14] Richards, A., Schouwenaars, T., How, J. P., and Feron, E., “Spacecraft Trajectory Planning with Avoidance Constraints Using Mixed-Integer Linear Programming,” *Journal of Guidance, Control, and Dynamics*, Vol. 25, No. 4, 2002, pp. 755–764,
doi:<https://doi.org/10.2514/2.4943>.
- [15] Breger, L. and How, J. P., “Safe Trajectories for Autonomous Rendezvous of Spacecraft,” *Journal of Guidance, Control, and Dynamics*, Vol. 31, No. 5, 2008, pp. 1478–1489,
doi:<https://doi.org/10.2514/1.29590>.
- [16] Deaconu, G., Louembet, C., and Thérion, A., “Designing Continuously Constrained Spacecraft Relative Trajectories for Proximity Operations,” *Journal of Guidance, Control, and Dynamics*, Vol. 38, No. 7, 2015, pp. 1208–1217,
doi:<https://doi.org/10.2514/1.G000283>.
- [17] Weiss, A., Baldwin, M., Erwin, R. S., and Kolmanovsky, I., “Model Predictive Control for Spacecraft Rendezvous and Docking: Strategies for Handling Constraints and Case Studies,” *IEEE Transactions on Control Systems Technology*, Vol. 23, No. 4, 2015, pp. 1638–1647,

doi:<https://doi.org/10.1109/TCST.2014.2379639>.

- [18] Leomanni, M., Rogers, E., and Gabriel, S. B., “Explicit Model Predictive Control Approach for Low-Thrust Spacecraft Proximity Operations,” *Journal of Guidance, Control, and Dynamics*, Vol. 37, No. 6, 2014, pp. 1780–1790,

doi:<https://doi.org/10.2514/1.G000477>.